Cement and Concrete Research 40 (2010) 971–983

Contents lists available at ScienceDirect

Cement and Concrete Research

journal homepage: http://ees.elsevier.com/CEMCON/default.asp

Composition and microstructure of 20-year-old ordinary Portland cement–ground granulated blast-furnace slag blends containing 0 to 100% slag

R. Taylor [a,b], I.G. Richardson [a,*], R.M.D. Brydson [b]

[a] School of Civil Engineering, University of Leeds, Leeds LS2 9JT, United Kingdom
[b] Institute for Materials Research, University of Leeds, Leeds LS2 9JT, United Kingdom

ARTICLE INFO

Article history:
Received 10 October 2008
Accepted 22 February 2010

Keywords:
Portland cement (D)
Granulated blast-furnace slag (D)
C–S–H (B)
TEM (B)
NMR

ABSTRACT

The morphology of outer-product (Op) C–S–H in 20-year-old slag–cement pastes appeared in most blends to be finer than at younger ages. The Ca/Si and Ca/(Si + Al) ratios of the Op C–S–H decreased with increasing slag content, and the Al/Si ratio increased. The Ca/Si ratio of C–S–H in the slag-containing pastes was lower at 20 years than at 14 months and the amount of $Ca(OH)_2$ was reduced indicating that additional slag must have reacted. The mean aluminosilicate chain length of the C–S–H was very long in all the samples and would be expected to have increased with age. The TEM-EDX and NMR data are consistent with nanostructural models for C–S–H. The Mg/Al ratio of the Mg–Al layered double hydroxide phase (LDH) was lower at 20 years than at 14 months in all cases except for the neat slag paste; aluminium hydroxide-based structure might be interstratified with those of the Mg–Al LDH.

1. Introduction

The majority of research on the microstructure of cementitious materials involves hydration periods of up to perhaps three years, which is the maximum age possible in a typical PhD project. The service life of concrete structures is of course much longer than this, and the materials used to encapsulate intermediate level radioactive wastes must be effective over extremely long timescales. It is therefore important to know if significant changes occur to the microstructure of hardened cements over periods beyond three years, and, in particular, if the nature of the main binding phase is affected, which in all Portland cement-based systems is a calcium silicate hydrate (C–S–H). The chemical composition, morphology and nanostructure of C–S–H are known to be very variable, being influenced by many factors, including the composition of the cement, the water to cement ratio, the curing temperature, the degree of hydration, and the presence of chemical admixtures and supplementary cementing materials (SCM) [1]. Ground granulated blast-furnace slag (GGBS) is a widely used SCM that is blended with ordinary Portland cement (OPC) at replacement levels of up to 90% slag. Although there are many publications concerning various aspects of blended cements that incorporate GGBS (some of which are discussed in [1]), there have been few studies on the nature of the C–S–H in such systems, and none that concern C–S–H present in mature samples, other than the paper that reports the first results from the current work [2]. The composition and morphology of C–S–H in 14-month-old samples of varying GGBS/OPC ratio have been characterized by transmission electron microscopy (TEM) [3], and samples from the same batches were extant at the outset of the current study. The purpose of this work was, therefore, to examine the nature of C–S–H in those 20-year-old samples and compare the results with data on the same mixes at 14 months old [3]. The samples were examined using ^{29}Si and ^{27}Al magic angle spinning (MAS) nuclear magnetic resonance spectroscopy (NMR), X-ray diffraction, thermal analysis with evolved gas analysis, and analytical TEM.

2. Experimental

The oxide compositions that were supplied with the anhydrous OPC and GGBS are given in Refs. [2,3]. The slag was largely glassy with a small amount of melilite. The composition of the slag glass was determined by electron microprobe analysis of powder, embedded in resin, ground and polished flat. The microprobe was a Cameca Camebax (operating voltage of 15 kV and probe current of 3×10^{-8} A) and the data were collected using wavelength dispersive spectrometers. In total, 392 particles were analysed with the following results (mean atom ratio ± 1 standard deviation): Ca/Si = 1.09 ± 0.06, Ca/(Al + Si) = 0.80 ± 0.04, Al/Si = 0.37 ± 0.02, and Mg/Si = 0.32 ± 0.02.

Pastes were prepared by mixing the required amounts of solids with de-ionised water at a water to solids ratio of 0.4 (ml/g). The samples were cast in plastic tubes, sealed in polyethylene bags and cured in a water bath at 20 °C from 1986 to December 1994 after which they were removed from the water bath and simply stored – still sealed in the tubes and bags – in the ambient conditions of an office at the University of Leeds. Data collected on samples aged 14 months have been published in Refs. [3,4]. The experimental details for the techniques used to examine the 20-year-old samples in the current work are

* Corresponding author.
E-mail address: I.G.Richardson@leeds.ac.uk (I.G. Richardson).

0008-8846/$ – see front matter © 2010 Elsevier Ltd. All rights reserved.
doi:10.1016/j.cemconres.2010.02.012

described in the previous paper [2]. In addition to those techniques, ^{27}Al MAS NMR spectra were collected at a field strength of 9.4 T (operating frequency of 104.2 MHz for ^{27}Al; spinning speed 14.0 kHz; no ^{1}H decoupling) using a pulse delay of 0.2 s, a pulse width of 1.0 μs and an acquisition time of 10 ms, for 10,000 repetitions. The samples were spun for no longer than 40 min in order to prevent dehydration of the sample and any consequent loss in intensity of peaks [5]. The extent of slag reaction in each paste was estimated by comparing the intensity of the peak due to glassy slag determined from the deconvolution of the single-pulse ^{29}Si NMR spectrum of the paste with that from the corresponding anhydrous blend, which was acquired using the same experimental parameters (anhydrous material had been kept for 20 years as well as the pastes). A Voigt analytical peak shape was used to fit the slag resonance, which was found to give acceptable fits, although there was some variation in peak shape between pastes; this is in contrast with previous work where the use of Voigt peaks gave values for unreacted slag that were higher than in the anhydrous material and were thus clearly incorrect (Method 2 in Ref. [6]).

3. Results and discussion

3.1. X-ray diffraction and thermal analysis

X-ray diffraction traces for the neat cement paste and the blends are shown in Fig. 1, together with schematic diagrams for relevant phases. The data are all plotted with the same intensity scales. The crystalline phases present in the neat cement paste included CH, AFt, hydrogarnet, a small amount of residual cement (including calcium aluminoferrite), a small amount of calcite and possibly some AFm that contains carbonate ions. The presence of the last two indicates that the neat paste was very slightly carbonated. The blended pastes contained progressively smaller amounts of CH as the slag fraction increased, and a hydrotalcite-like phase (i.e. a Mg–Al layered double hydroxide (Mg–Al LDH)). Thermal analysis techniques combined with analysis of the evolved gases were used to complement the XRD data. An example of these data is given in Fig. 2, which is for the blend containing 50% slag; the loss of mass below 400 °C is due to the decomposition of the C–S–H, AFm and Mg–Al LDH phases, and the sharp loss between 400 and 500 °C is due to CH. The mass spectroscopy data showed that no carbon dioxide was evolved during the thermal analysis experiments other than a very small amount for the neat cement paste, indicating that none of the slag-containing pastes had carbonated, which is in agreement with the XRD results. The amount of calcium hydroxide in the blends is given in Table 1, together with the amount as a percentage of the value expected on the basis of simple dilution, R^{20y}; in all cases R^{20y} is much less than 100%, which indicates that less calcium hydroxide is present than expected on that basis, due to the reaction of the glassy slag to produce C–S–H. R^{20y} is also less than the equivalent value at 2 years (R^{2y}) in all the blends, which is consistent with additional slag reaction occurring between 2 and 20 years; the 2-year data are from Ref. [7].

3.2. ^{29}Si MAS NMR

Fig. 3 shows the single-pulse ^{29}Si MAS NMR spectra – and the results of the deconvolution of the spectra – for all the pastes except for the neat cement, which is presented and discussed in Ref. [2]; the spectrum for the blend containing 90% slag was also presented in that paper but the deconvolution procedure has been repeated using an additional peak (see discussion below). The broad peak on the spectra that has a chemical shift at about −73 ppm is mainly due to unreacted glassy slag, although there is likely to be a small peak due to hydrated monomer (Q^{0H}) in some of the pastes that is essentially superposed on the slag peak. The −73 ppm peak is particularly intense in the spectrum for the neat slag, indicating that a large amount of slag has remained unreacted, which is consistent with the slow rate of reaction of unactivated slag.

The spectra were initially fitted using three peaks for the C–S–H (Q^1, Q^2(1Al) and Q^2(0Al) at approximately −79, −81.5 and −85 ppm respectively) but this was not satisfactory for the pastes with 50, 75 and 100% slag because the Al/Si ratio calculated using the deconvoluted peak intensities was much higher than that measured directly by

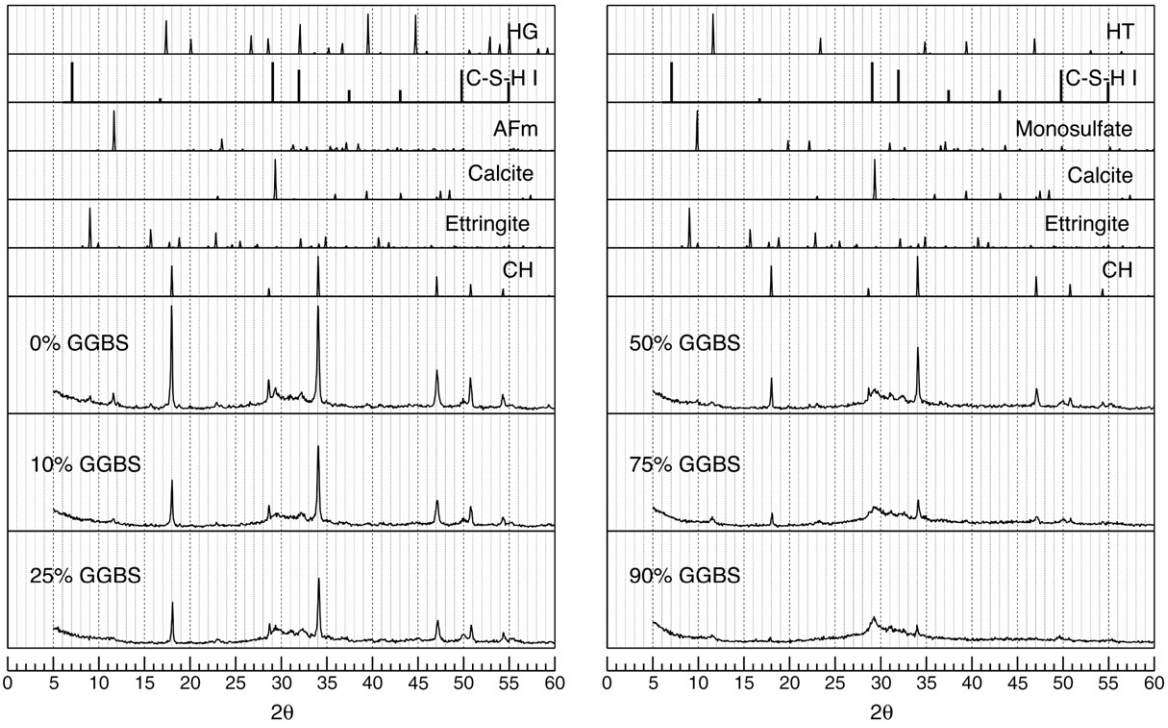

Fig. 1. X-ray diffraction traces for the pastes containing 0, 10, 25, 50, 75 and 90% slag. Schematic X-ray powder diagrams are included for relevant phases: HT = hydrotalcite; HG = hydrogarnet. The data are all plotted with the same intensity scales.

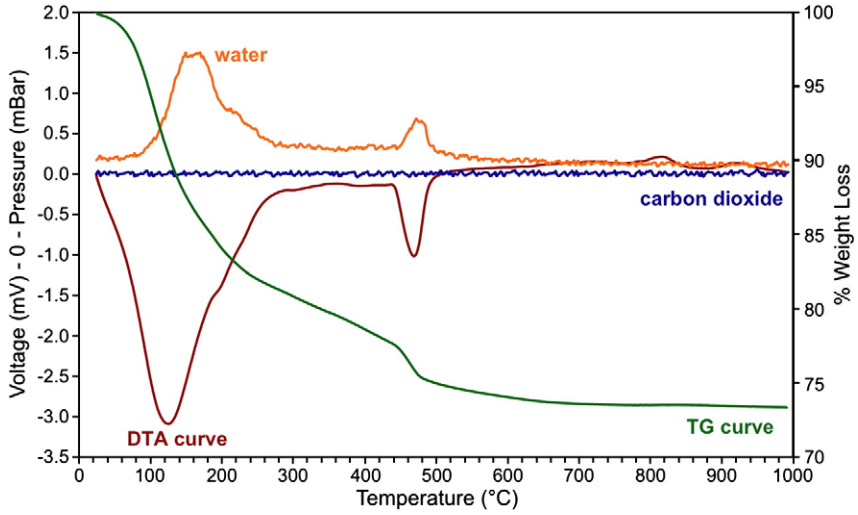

Fig. 2. Thermal analysis data for the paste containing 50% slag.

TEM-EDX (see Section 3.4), which is in contrast with results for a number of other systems (for example see Fig. 17 in Ref. [8]). The difference between the two values can be reduced by the inclusion of a fourth C–S–H peak that has a similar chemical shift to Q^2(1Al) but which is not associated with aluminium (since this has the effect of reducing the NMR Al/Si ratio). Peaks within the appropriate chemical shift range have been observed in samples of aluminium-free synthetic C–S–H, for example by Klur et al [9] who considered them to be due to 'bridging' tetrahedra in dreierkette silicate chains, i.e. additional Q^2 species, which they labelled Q^{2p} or Q^{2i}, depending upon the suggested local chemical environment. Q^{2B} is used as a label in this work for the fourth C–S–H peak but it must be emphasized that intensity due to bridging tetrahedra must also be present in the main Q^2 peak (otherwise, for example, the C–S–H in the neat cement paste – where a Q^{2B} peak is not needed – could not have silicate chains with dreierkette conformation). Unfortunately, because of the limited resolution of the spectra in Fig. 3, the only way that the fourth peak could be incorporated meaningfully was to simply allocate a proportion of the Q^2(1Al) peak to Q^{2B} such that the Al/Si ratio calculated from the deconvoluted peak intensities was the same as that measured by TEM-EDX (the Al/Si of the Op C–S–H was used although the results of the regression analysis of the data for slag inner product indicate that the average value for all the C–S–H in some of the blends might be lower, Section 3.4). The results from the deconvolution of the spectra are given in Tables 1 and 2: Table 2 summarizes the chemical shifts of the hydrate peaks and Table 1 includes the percentages of cement and slag reacted, the mean aluminosilicate chain length (MCL) of the C–S–H and its Al/Si ratio (which is, of course, the same as measured by TEM-EDX for five of the blends).

Inspection of Fig. 3 reveals a striking reduction in the intensity of the Q^1 peak (i.e. in chain-end groups) as the slag loading increases, which translates as a dramatic increase in the mean length of the aluminosilicate anions (MCL, Table 1). Unfortunately, the MCL in the C–S–H present in these pastes at 14 months was not determined; however, the MCL in similar systems is much shorter at younger ages (e.g. 3.4 in a 2-year-old neat OPC paste [10] and 6.5 in a 3-week-old GGBS–OPC paste containing 90% slag [11]), which suggests that the MCL will have increased in all systems as a result of sample age. The proportion of bridging tetrahedra in the dreierkette chains that contain Al^{3+} rather than Si^{4+} (B in Table 1) is quite similar for most of the blends, varying between 42 and 53%.

The degree of reaction of the silicate phases in the Portland cement fraction of the pastes was high in all cases, with only small amounts of residual belite present (Fig. 3 and Table 1). Whilst the percentages of slag reacted given in Table 1 must be considered approximate, the results nevertheless indicate that around two thirds of the glassy slag appears to have reacted in the blends with ≤75% slag, about a third in the blend with 90% slag, and just a fifth in the neat slag paste.

Table 1
Results from thermal analysis and the deconvolution of the single-pulse ^{29}Si NMR spectra for the neat and blended cement pastes. MCL = mean aluminosilicate chain length for C–S–H; B = bridging tetrahedra occupied by Al/bridging tetrahedra occupied by Al and Si. % CH = calcium hydroxide as % of ignited weight determined by thermogravimetry; $\%\,CH^{exp.} = \%\,CH \times$ fraction OPC in the paste. R^{20y} is the amount of CH in the blends as a percentage of the value expected on the basis of simple dilution; R^{2y} is the corresponding percentage after about 2 years hydration (the 2-year data are from Ref. [7]).

% GGBS in paste	% CH	% CH^{exp}	R^{20y}	R^{2y}	Al/Si	MCL	B (%)	% cement reacted	% slag reacted
0	28	28	100	100	0.08	5.6	33	96	–
10	18	25	72	91	0.12	6.7	47	97	77
25	12	21	57	87	0.11	7.1	42	100	67
50	10	14	71	76	0.14	13.8	43	98	68
75	3	7	43	68	0.16	16.1	47	94	60
90	1	3	33	43	0.18	14.3	53	100	36
100	0	0	–	–	0.19	∞	50	–	22

3.3. ^{27}Al MAS NMR

^{27}A1 MAS NMR spectra can be difficult to interpret because of the quadrupolar interaction, which leads to a field-dependent shift in resonance position and a broadening of the peaks that can result in severe overlap [12]. Resonances for aluminium that is in 4-fold coordination to oxygen atoms ($Al^{[4]}$) are generally observed in the range 50 to 80 ppm and those for 6-fold coordination ($Al^{[6]}$) in the range −10 to 20 ppm; chemical shifts for penta-coordinated Al ($Al^{[5]}$) are intermediate between $Al^{[4]}$ and $Al^{[6]}$. The single-pulse ^{27}Al MAS NMR spectra for the 20-year-old pastes are shown in Fig. 4. The main aluminium environments are octahedrally coordinated, with three peaks between 0 and 20 ppm; there are generally relatively minor amounts of tetrahedral aluminium, (indicated by a broad peak at around 65 ppm) and penta-coordinated aluminium (a small peak at around 35 ppm). The 65-ppm peak is due to unreacted glassy slag [13,14] and there is also a contribution in this region from tetrahedrally coordinated aluminium in the C–S–H. The three octahedral peaks are at approximately 13, 9 and 4 ppm. The peak at ≈13 ppm is assigned to an AFt phase [15,16], which is known to be present from XRD and TEM. It seems probable that the peak at ≈9 ppm is a convolution of resonances from an AFm phase [15] and a Mg–Al LDH phase, both of which are also known to be present from

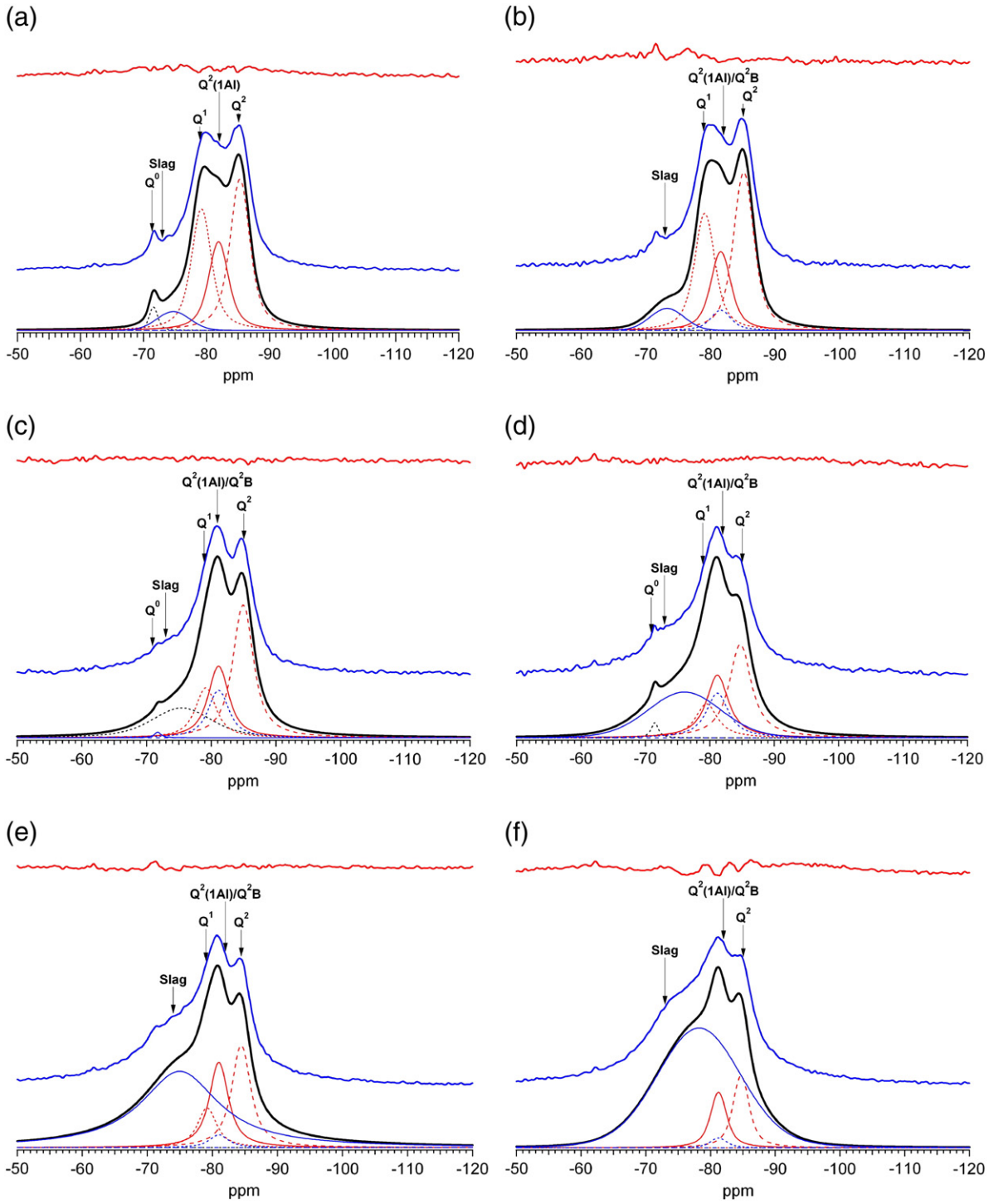

Fig. 3. Single-pulse ^{29}Si MAS NMR spectra for pastes with (a) 10, (b) 25, (c) 50, (d) 75, (e) 90, and (f) 100% GGBS (magnetic field 7.05 T; spinning speed 6 kHz; pulse recycle delay 2 s; pulse width 4 ms; acquisition time 20 ms). The spectra are scaled to their tallest peak. The figures include the experimental spectrum (middle), the fitted peaks (bottom), and the residual (top; ×1). The chemical shifts of the hydrate peaks (in ppm) are given in Table 2. The larger of the two superposed peaks at ≈−81.5 ppm is $Q^2(1Al)$ and the other is Q^{2B}.

XRD and TEM: a chemical shift of ≈9 ppm has been reported in studies at the same field for hydrotalcite-type phases [17–19] and for monosulfate [16]. A third octahedral peak has been observed previously in hardened Portland cement pastes, which could not be assigned to any of the well-known aluminate species [20]. Andersen et al. concluded that the peak – which was at 4.1 ppm at the field strength used in this work – was due to an amorphous or disordered aluminate hydrate, which they denoted as the 'third aluminate hydrate' (TAH) [20]. Whilst Andersen et al. observed no correlation between the quantity of TAH formed in neat cement pastes with the bulk Al_2O_3 content of the cement [20], the intensity of the $Al^{[6]}$ resonance at ≈4 ppm in Fig. 5 does appear to increase with bulk Al_2O_3 content (because the Al_2O_3 content of the slag is greater than that of the cement); a plausible reason for this observation is discussed in Section 3.4.

3.4. Transmission electron microscopy with X-ray analysis

The most distinctive feature of the neat cement paste is the fineness of the morphology of outer-product (Op) C–S–H [2], which

Table 2
^{29}Si chemical shifts for the hydrate peaks (in ppm).

% GGBS in paste	Q^1	$Q^2(1Al)/Q^{2B}$	$Q^2(0Al)$
0	−78.9	−81.9	−84.9
10	−79.2	−81.9	−85.3
25	−79.1	−81.6	−85.1
50	−79.2	−81.2	−84.9
75	−79.5	−81.2	−84.7
90	−79.2	−81.0	−84.4
100	–	−81.2	−84.7

appears to be finer than at younger ages [4]. This is also true for many of the samples that contain slag: Fig. 5, for example, shows a region of very fine C–S–H in the paste that contains 10% slag; indeed, regions of Op C–S–H were sufficiently fine in most of the pastes that it was often difficult to distinguish between Op and Ip when examining the samples in the microscope. In this paste, as in the neat cement paste (see Fig. 4 of Ref. [2]), the fibrils of C–S–H appear to consist of agglomerations of particles of varying length that are around 5 nm in their smallest dimension.

There is a progressive change in morphology of the Op C–S–H as the amount of slag in the blend increases, essentially changing from fibrillar to foil-like; this was also observed at 14 months [2], although after 20 years – as noted above – the fibrillar morphology is generally finer. Fine Op C–S–H is present on the left-hand-side of Fig. 6 (25% slag), with an enlargement shown in Fig. 7; the striations are relicts of AFt. C–S–H with fine-fibrillar morphology is also present in much of Fig. 8 (50% slag), although in that case its designation as outer product is debatable given that in many instances it surrounds laths of the Mg–Al LDH phase, which at younger ages are only found in inner product regions [3]. Similarly fine Op C–S–H is also present in the paste containing 75% slag (Fig. 9). Whilst some fibrillar Op C–S–H was also present in the paste with 90% slag, it was largely foil-like, and essentially the same as it was at 14 months [2,3]. With 100% slag, the Op C–S–H consisted entirely of crumpled foils (Figs. 10 and 11); which was again the same as at

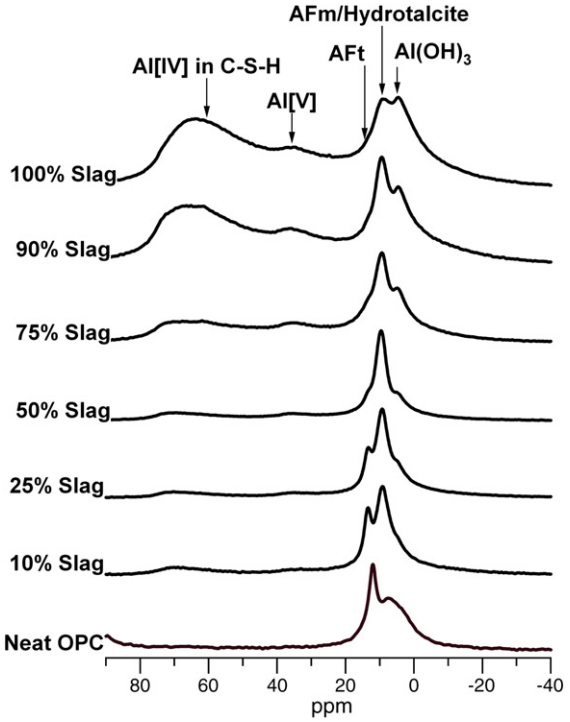

Fig. 4. ^{27}Al MAS NMR spectra for pastes with 0, 10, 25, 50, 75, 90 and 100% GGBS. The spectra are plotted with the same intensity scale.

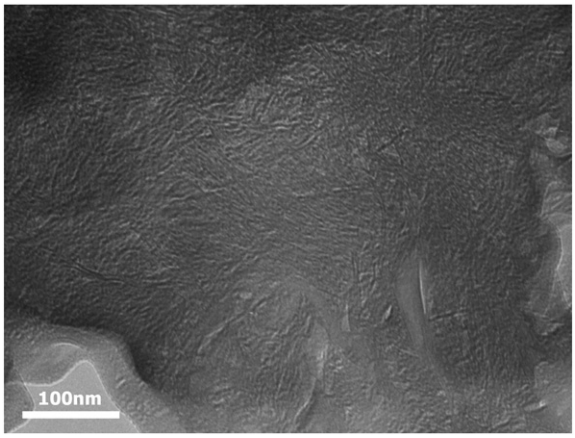

Fig. 5. A TEM micrograph that illustrates fine, dense C–S–H in the paste containing 10% slag.

14 months [3]. The particle size-related variation in morphology of inner product C–S–H that was noted at younger ages [3,4] was still observed in these 20-year-old pastes: i.e. a fine, dense morphology around partly reacted grains but a coarser, foil-like morphology where there was no residual unreacted cement; a good example is present at the top of Fig. 6. The presence of CH crystals in the majority of the samples and some laths of the Mg–Al LDH phase is in agreement with XRD and thermal analysis results.

Areas of Op C–S–H and inner product in all the pastes were analysed by EDX in the TEM (≈200 nm in diameter). Each region for analysis was first checked by selected area electron diffraction (SAED) for the presence of crystalline phases that might be intermixed with the C–S–H. The numbers of analyses taken are given in Table 3 together with the mean values and standard deviations of the Ca/Si ratio for both Op and Ip, and the Ca/(Si + Al) and Al/Si ratios for Op C–S–H. Some of the analyses that were nominally of C–S–H were excluded from the statistical analysis on the basis of compositional trends that suggested a contribution from a phase other than C–S–H, such as AFt, which is very unstable in the electron beam (and as a consequence it is not revealed by SAED). The analyses that correspond to more than one

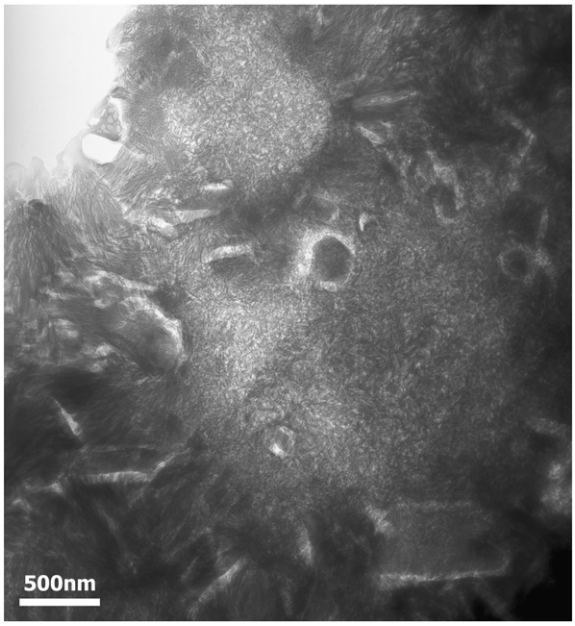

Fig. 6. A TEM micrograph that illustrates fine, dense Op C–S–H, Ip C–S–H and AFt relicts in the paste containing 25% slag.

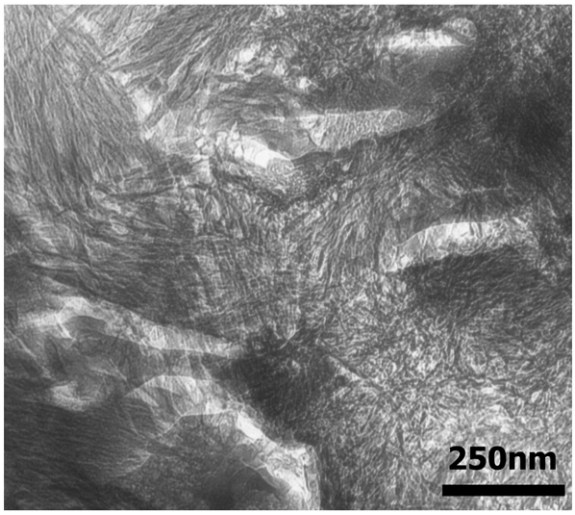

Fig. 7. An enlargement of a region of Fig. 6 that shows intermixing of C–S–H and relicts of AFt.

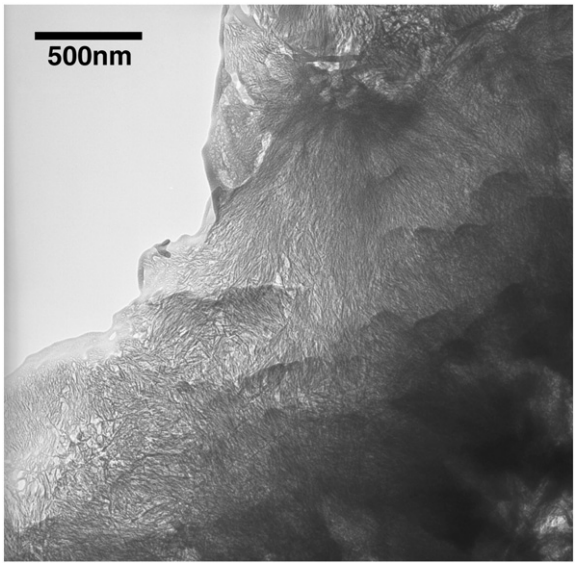

Fig. 9. A TEM micrograph that illustrates fine, dense Op C–S–H in the paste containing 75% slag.

phase are evident in Figs. 12–16, which are Al/Ca against Si/Ca scatter graphs of the TEM-EDX data for the pastes with 10, 25, 50, 75 and 100% slag (the equivalent plots for the 0 and 90% pastes are given in Ref. [2]), and in Fig. 17, which includes Mg/Si against Al/Si scatter graphs for the same pastes. The plots in Fig. 17 clearly demonstrate that the slag inner product in these pastes consists of a mixture of C–S–H with varying amounts of a Mg–Al LDH phase: the gradient of the linear regression line is the Mg/Al ratio of that phase; the Al/Si ratio of the C–S–H that is mixed with it, which is the value at Mg/Si = 0, is lower than the value for the Op C–S–H in a number of the blends (Table 3). The regression analysis included all analyses that contain the Mg–Al LDH phase, regardless of whether they were originally identified morphologically as Ip or Op (it was, as noted above, often difficult to decide whether a region was Ip or Op); for convenience, all such analyses are included in the table as Ip, but are displayed in Figs. 12–17 with the symbol appropriate for the original morphological identification. The fact that inner product consists of a mixture of two phases that both contain aluminium is the reason why the Ca/(Si + Al) ratio is not given in Table 3 for Ip C–S–H.

The inaccuracy of the Al/Si ratios for the pastes containing 50, 75 and 100% slag derived from the NMR data without the use of a fourth C–S–H peak (see Section 3.2) is confirmed by inspection of the TEM-EDX data for the neat slag paste. A balance for the main cations – Ca^{2+}, Si^{4+}, Al^{3+}, and Mg^{2+} – for that paste should be straightforward if the chemical compositions of all the phases have been determined correctly, because those ions are present in only one reactant (the glassy slag), the calcium and silicon ions are only present in one of only two products (C–S–H), and magnesium is only present in the other product (the Mg–Al LDH;

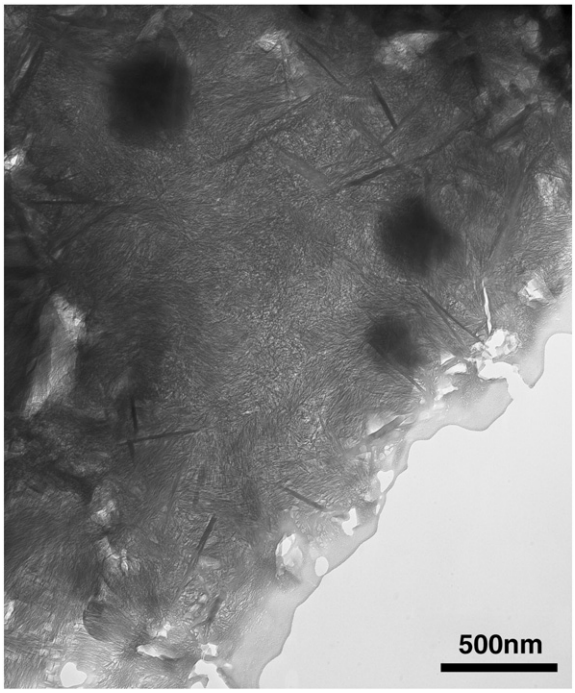

Fig. 8. A TEM micrograph of a region in the paste containing 50% slag that illustrates fine C–S–H intermixed with laths of a Mg–Al LDH phase.

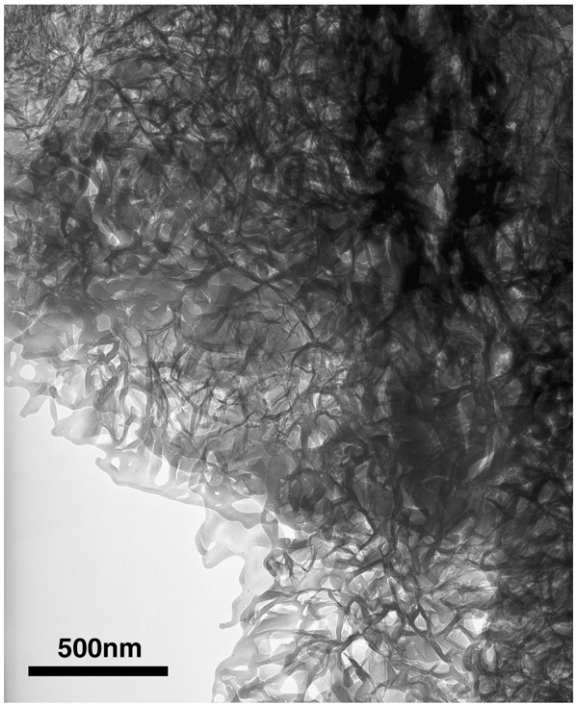

Fig. 10. A TEM micrograph that illustrates foil-like Op C–S–H in the neat slag paste.

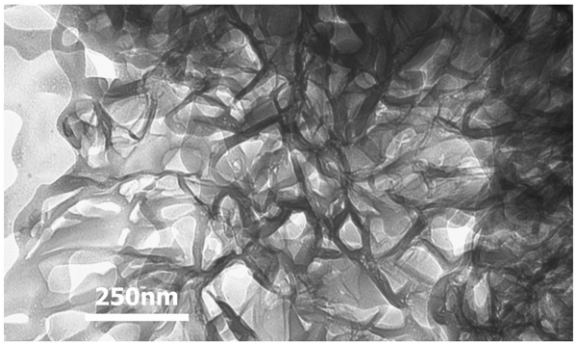

Fig. 11. An enlargement of a region of Fig. 10 that shows foil-like Op C–S–H.

there is no Mg present in the C–S–H, Fig. 17). This means that the mean Ca/Si ratio of the C–S–H (that was determined by TEM-EDX) should be the same as that for the glassy slag (determined by EMPA), which is indeed the case ($Ca/Si^{slag} = 1.09 \pm 0.06$ ($N = 392$); $Ca/Si^{C-S-H} = 1.08 \pm 0.06$ ($N = 59$)). The relative amounts of the C–S–H and Mg–Al LDH phase can be determined easily (because the former is the only product that contains calcium and silicon and the latter magnesium). The values determined by TEM-EDX for the Mg/Al ratio of the Mg–Al LDH phase (1.79) and for the Al/Si ratio of the C–S–H (0.19) are entirely consistent with the composition of the glassy slag determined by EMPA (which is given in Section 2). The overall reaction can be summarized in oxide notation as follows (for simplicity, it is assumed that the interlayer anions in the Mg–Al double hydroxide are all OH^-, as in the mineral meixnerite, which is $[Mg_6Al_2(OH)_{16}](OH)_2 \cdot 4H_2O$, or M_6AH_{13}):

$$C_{1.09}SA_{0.185}M_{0.32} + xH \rightarrow C_{1.09}SA_{0.095}H_y + 0.09M_{3.58}AH_z \quad (1)$$

Slag glass water C–S–H Mg–Al LDH.

The consistency of the compositions measured for the slag glass, C–S–H and Mg–Al LDH indicates that the Al/Si ratio of the C–S–H determined by TEM-EDX is correct, and that the value calculated from the NMR spectrum fitted with three C–S–H peaks is therefore too high.

As expected, the Ca/Si and Ca/(Si + Al) ratios of the Op C–S–H decrease with increasing slag content, and the Al/Si ratio increases. The Ca/Si ratio of Op C–S–H in the neat paste is higher at 20 years [2] than at 14 months [4], and the value for Ip C–S–H is about the same. In contrast, the values for both Op and Ip C–S–H in the slag-containing pastes are all lower at 20 years than they were at 14 months, Fig. 18; the difference is statistically significant in most cases. Perhaps surprisingly, there are good linear correlations between the two ages: the full lines in Fig. 18 are linear regression fits for the slag-containing blends: (a) for Op C–S–H, $Ca/Si_{20y} = 0.290 + 0.703(Ca/Si_{14m})$, $r^2 = 0.95$; (b) for inner product, $Ca/Si_{20y} = 0.325 + 0.662(Ca/Si_{14m})$, $r^2 = 0.97$.

The Mg/Al ratio of the Mg–Al LDH phase is essentially unchanged with time in the neat slag paste, but in all other cases it is much reduced: Fig. 19 shows a comparison of the Mg/Al ratio at 20 years and at 14 months in the pastes containing 10%, 25%, 50%, 75%, 90% and 100% slag; the data for the 20-year-old pastes are given in Table 3 and those for 14 months are as reported in Ref. [3]. At 14 months the value was above 2 in all cases except for the neat slag paste, but at 20 years all but the paste containing 10% slag has a ratio ≤2, which means that in most of the pastes the Mg/Al ratio is either the same as, or less than, the probable minimum value possible for hydrotalcite-like phases (i.e. 2, [21,22]); as an example, whilst hydrotalcite itself has a Mg/Al ratio of 3 ($[Mg_6Al_2(OH)_{16}]CO_3 \cdot 4H_2O$), another Mg–Al carbonate LDH, quintinite, has a ratio of 2 (i.e. the probable minimum value, $[Mg_4Al_2(OH)_{12}]CO_3 \cdot 3H_2O$ [23]). We noted in Ref. [2] that a plausible explanation for this observation is that there are layers of $Al(OH)_3$-based structure interstratified with those of the Mg–Al double hydroxide. This explanation is supported by the ^{27}Al NMR results in Fig. 4, which show that the intensity of the $Al^{[6]}$ resonance at ≈4 ppm appears to increase as the slag content increases: increased intensity of the 4 ppm peak thus coincides with a reduction in the Mg/Al ratio of the Mg–Al LDH phase (Table 3 and Fig. 17). At first sight, the assignment of the peak at ≈ 4 ppm is not consistent with ^{27}Al NMR

Table 3
Mean Ca/Si, Ca/(Al + Si), and Al/Si atom ratios for C–S–H in all the cement pastes obtained using TEM-EDX (N = number of analyses; S.D. = standard deviation), and the Al/Si ratio determined by deconvolution of the single-pulse ^{29}Si MAS NMR spectra when fitted using three ('No Q^{2B}') or four C–S–H ('With Q^{2B}') peaks.

			Ca/Si		Ca/(Al + Si)		Mg/Al[a]	Al/Si			
								TEM		NMR	
% GGBS		N	Mean	S.D.	Mean	S.D.		Mean	S.D.	No Q^{2B}	With Q^{2B}
0	Op	47	1.84	0.15	1.68	0.13	–	0.10	0.03		
	Ip	10	1.67	0.12	1.54	0.11		0.08	0.01		
	All	57	1.81	0.16	1.66	0.14		0.09	0.03	0.08	
10	Op	53	1.60	0.18	1.40	0.19	2.17	0.15	0.06		
	Ip	24	1.60	0.25				0.03[b]			
	All	77	1.60	0.20						0.12	
25	Op	44	1.56	0.10	1.41	0.10	2.00	0.11	0.02		
	Ip	15	1.50	0.15				0.03[b]			
	All	59	1.55	0.12						0.13	0.11
50	Op	28	1.33	0.15	1.17	0.13	1.98	0.14	0.02		
	Ip	31	1.32	0.08				0.09[b]			
	All	48	1.32	0.12						0.20	0.14
75	Op	35	1.31	0.05	1.13	0.04	1.89	0.16	0.01		
	Ip	19	1.31	0.12				0.10[b]			
	All	54	1.31	0.08						0.23	0.16
90	Op	51	1.19	0.11	1.01	0.10	1.82	0.18	0.02		
	Ip	18	1.13	0.12				0.17[b]			
	All	69	1.18	0.11						0.20	0.18
100	Op	41	1.09	0.06	0.92	0.06	1.79	0.19	0.02		
	Ip	18	1.05	0.06				0.19[b]			
	All	59	1.08	0.06						0.23	0.19

[a] The Mg/Al ratio is the value for the Mg–Al LDH phase that is intermixed with C–S–H, which is derived from the regression analysis of the Mg/Si–Al/Si plots for all analyses that contain this phase, regardless of whether they were originally identified morphologically as Ip or Op; for convenience, all such analyses are included in the table as Ip, but are displayed in Figs. 12–17 with the symbol appropriate for the original morphological identification.
[b] The Al/Si ratio of the Ip C–S–H is the value determined from the regression analysis of the Mg/Si–Al/Si plots at Mg/Si = 0.

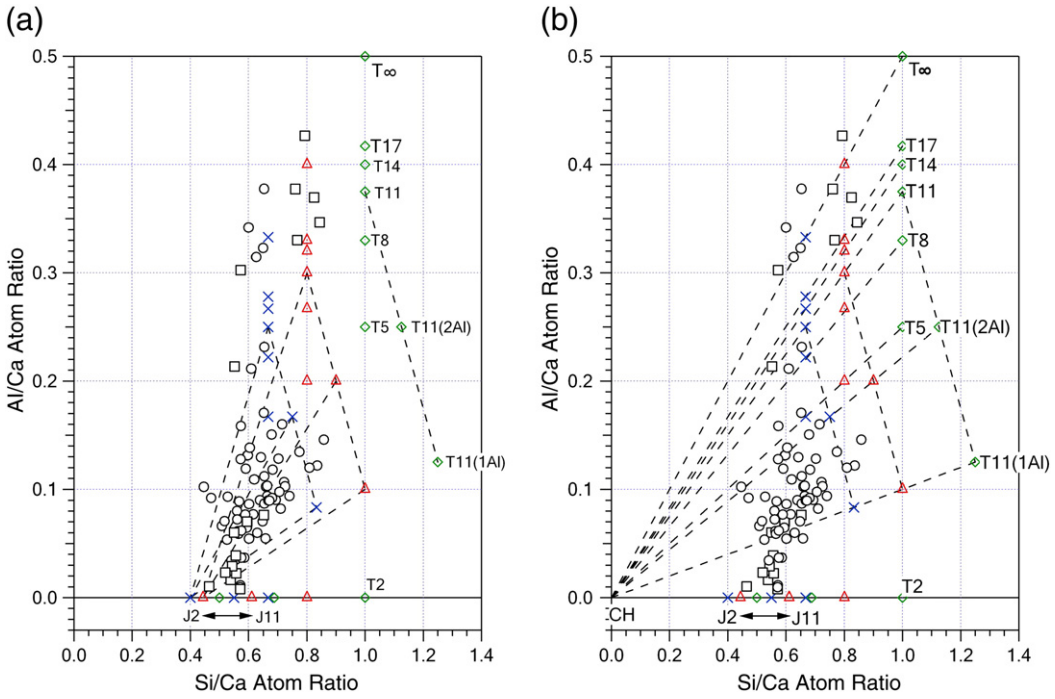

Fig. 12. (a) Al/Ca against Si/Ca atom ratio plot of TEM-EDX analyses of Ip (□) and Op (○) C–S–H present in the paste containing 10% slag. The other symbols represent the compositions of tobermorite- (T) or jennite-based (J) structural units with different levels of protonation of the silicate chains: the minimum level (◇; $w/n=0$), an intermediate level (Δ; $w/n=1$), and the maximum level (×; $w/n=2$). Points are included on the figures that represent tobermorite-based units with chain lengths of 2, 5, 8, 11, 14, 17 and ∞. Most of the units are saturated with Al (i.e. all the occupied bridging sites are occupied by Al rather than Si). The only exceptions are units with 11 tetrahedra, which in addition to those saturated with Al (i.e. Al/(Al + Si) = 3/11, which are labelled simply as T11), are also represented with one or two of the three bridging sites occupied by Al (i.e. Al/(Al + Si) = 1/11or 2/11): units with one or two Al ions are labelled as T11(1Al) and T11(2Al) respectively. T11 units with the same degree of protonation but different content of Al are joined by dashed lines. Dashed tie lines join points for T11 structural units with points on the Si/Ca axis that represent jennite-based dimer (with different degrees of protonation). (b) As (a) except that dashed tie lines now join points for structural units of the same length but different degrees of protonation with CH (at the origin).

studies of gibbsite, γ-$Al(OH)_3$. Gibbsite has two non-equivalent aluminium atoms, Al(1) and Al(2) [24]; the most prominent resonance on ^{27}Al MAS NMR spectra is due to one of the sites, Al(1) [15]. The isotropic chemical shift (δ^{iso}), quadrupolar coupling constant (C_Q) and asymmetry parameter (η) that have been determined for Al(1) using synthetic gibbsites [15,25] indicate that the resonance at the field used in this study (9.4 T) should be at a chemical shift of around 8 ppm, not 4 (the values given in Refs. [15,25] are similar, giving predicted shifts of 7.9 and 8.3 ppm respectively). The chemical shift expected at the lower field of 7.1 T is about 6 ppm, which is in good agreement with

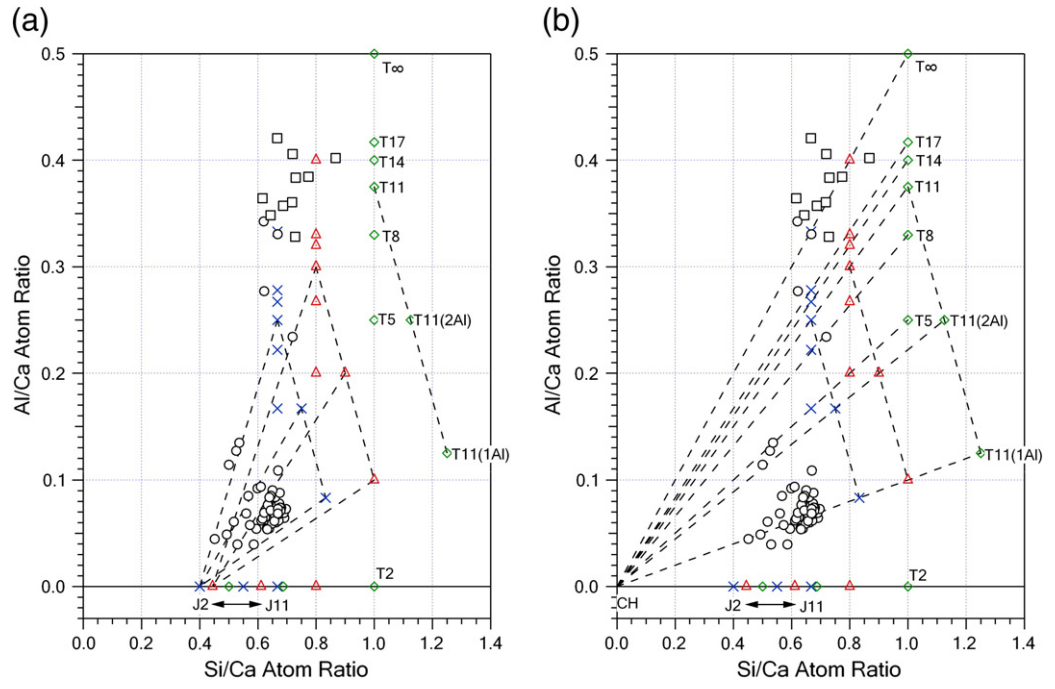

Fig. 13. As Fig. 12 but for the paste containing 25% slag.

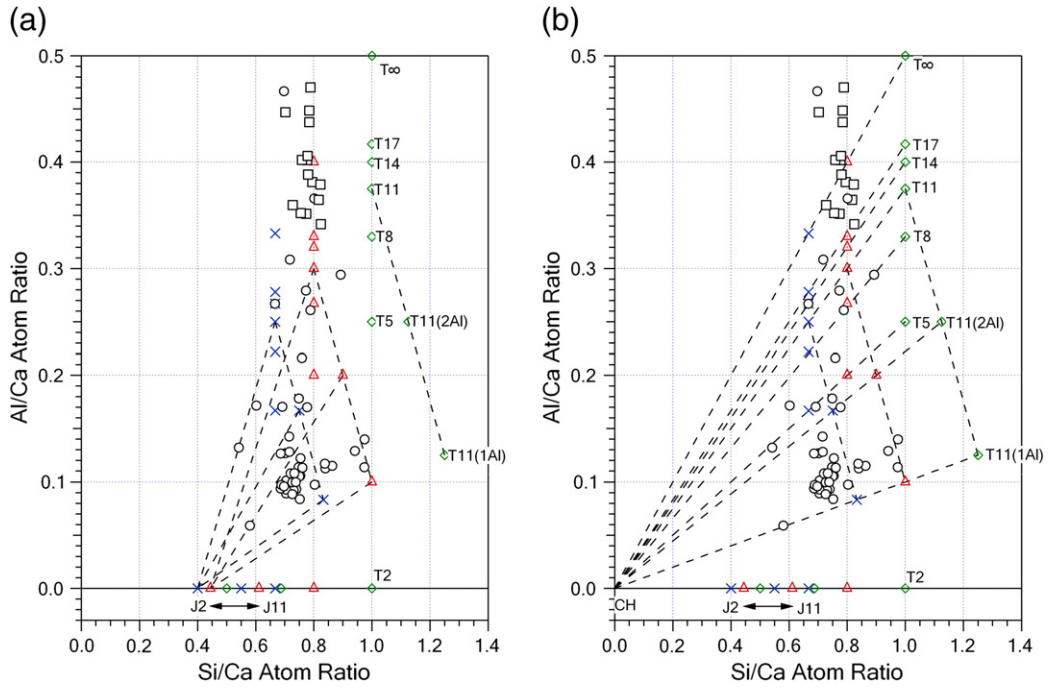

Fig. 14. As Fig. 12 but for the paste containing 50% slag.

the value observed by Slade et al. for one of two highly crystalline synthetic preparations (6.0 ppm) but not the second (4.7 ppm) [26]. In addition, Slade et al. also examined a natural gibbsite that was of 'lower crystallinity' than the synthetic preparations, which had a chemical shift of 4.4 ppm. It is therefore evident that the exact position of the Al(1) resonance at a given field is affected by the crystal size and degree of structural order of the gibbsite, so it is quite possible that the 4-ppm peak present in Fig. 4 is indeed due to poorly ordered layers of $Al(OH)_3$-based structure intermixed with those of the Mg–Al double hydroxide. If this assignment of the 4-ppm peak in these slag–cement blends is correct, then it seems plausible that similar layers could also occur in neat Portland cement pastes interstratified with layers of AFm, which is of course also a layered double hydroxide phase (that has a fixed M^{2+}/M^{3+} ratio of 2). It should be noted, however, that the $Al(OH)_3$-based structure cannot always be associated with an LDH phase since a 4-ppm peak has been observed as the only octahedral peak in spectra for some synthetic C–A–S–H preparations [27,28], although spectra for preparations with Ca/(Si + Al) ratios relevant to

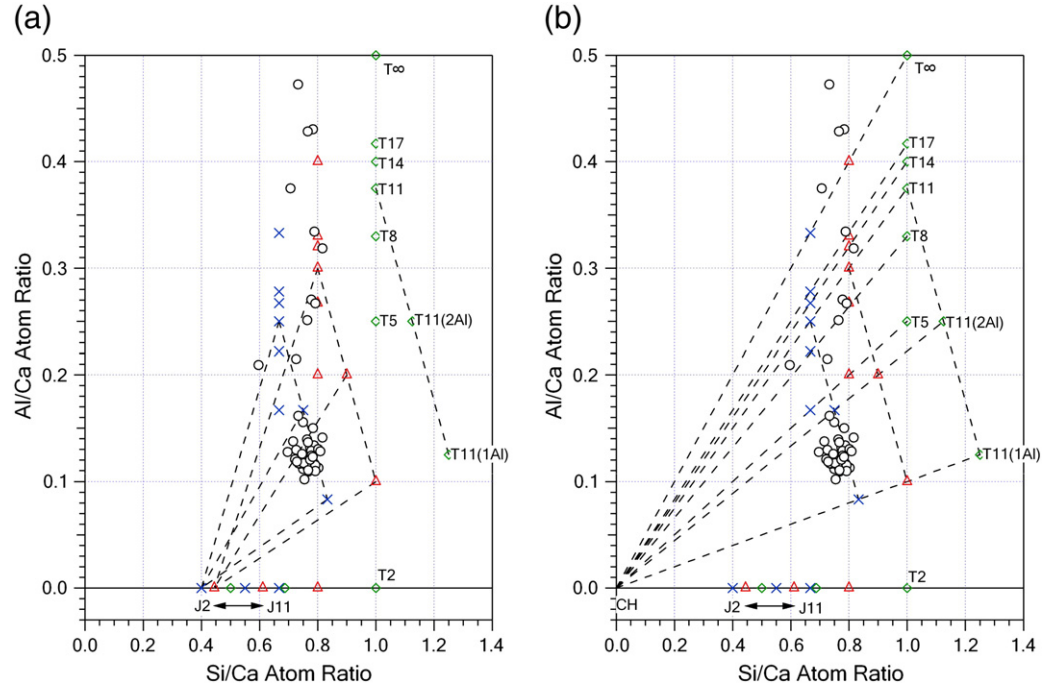

Fig. 15. As Fig. 12 but for the paste containing 75% slag.

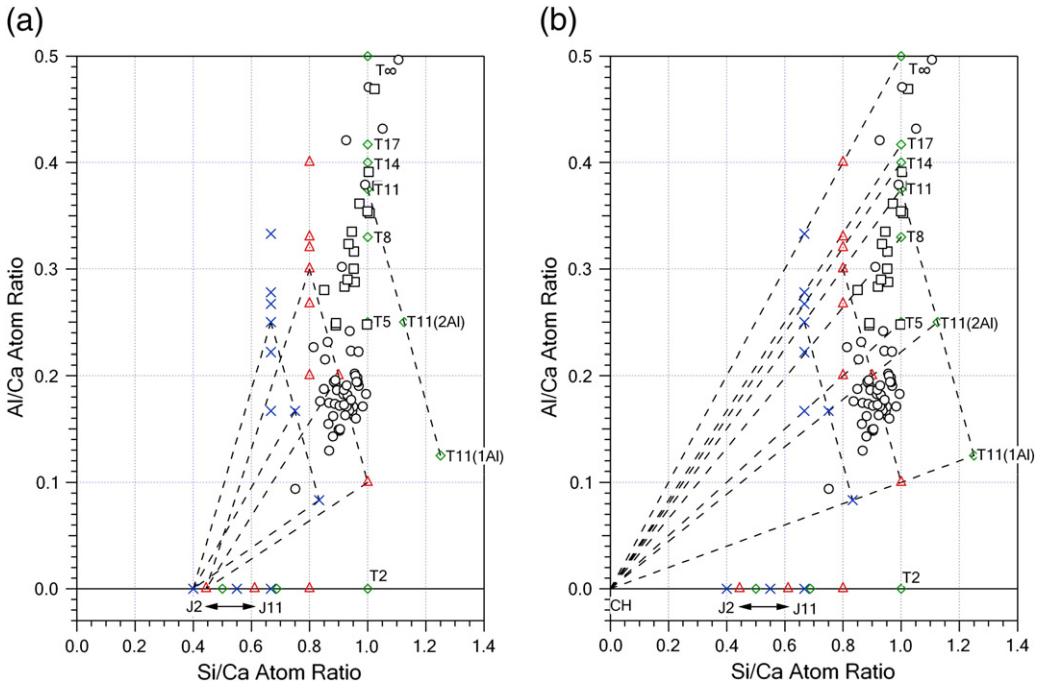

Fig. 16. As Fig. 12 but for the neat slag paste.

neat Portland cement pastes do in addition have a peak assigned to AFm [20].

3.5. Nanostructure of C–S–H

The results from the deconvolution of the ^{29}Si NMR spectra provide some information on the nature of the aluminosilicate anions in the C–S–H. Additional nanostructural insight can be obtained by comparing the distribution of the TEM-EDX analyses with the compositions of different units in Richardson and Groves' structural models [29,30]: points that represent various structural units are included in Figs. 12–16; an explanation of the different symbols and tie lines on the figures is given in the caption. The points for those units have been included to enable straightforward comparison with recent work on other systems [31–33] but there are of course many other structural units that have been omitted for the sake of clarity, some of which are particularly relevant to this discussion; details of those units are given in Table 4. The values of the mean aluminosilicate chain lengths and B (given in Table 1) should be noted before inspection of Figs. 12–16, and the positions of relevant structural units identified. The tie lines on the graphs that are on the left-hand side of the figures (i.e. Figs. 12(a)–16(a)) represent the T/J nanostructural viewpoint whilst those on the right-hand side (Figs. 12(b)–16(b)) represent the T/CH viewpoint. The relative positions of the TEM-EDX analyses and points representing the appropriate structural units (i.e. units based on the MCL and B, Table 1) are sensible. All the data for the paste containing 10% slag are compatible with T/J-based structure that has long-chain Al-substituted T units mixed with J-based dimer; since some of the data are also compatible with the T/CH viewpoint, it is possible that the C–S–H could consist of a mixture of T-, J- and CH-like structure. The NMR and TEM-EDX data can be used to establish structural–chemical formulae that represent average units in the C–S–H in terms of the T/J or T/CH viewpoints [30]; an example is given next for the paste containing 10% slag and values for the models' variables for the C–S–H present in the other blends are given in Table 5.

In terms of the T/J viewpoint, the C–S–H in the 10% slag paste is represented by (2), assuming a minimum degree of protonation of the aluminosilicate chains and that the substitution of Si^{4+} by Al^{3+} is balanced entirely by Ca^{2+} ions (the NMR Al/Si ratio is used since it lies intermediate between the TEM-EDX values for Op and Ip C–S–H):

$$\{Ca_{5.1}(Si_{0.89}A_{0.11})_{6.7}O_{21.1}\}\cdot(OH)_{3.03}\cdot Ca_{4.44}\cdot mH_2O \quad (2)$$

The presence of hydroxyl groups outside the braces indicates that in terms of the T/J viewpoint, there must be much J-like structure. In terms of the T/CH viewpoint, the average structural unit is represented by Eq. (3):

$$Ca_{7.7}(Si_{0.89}Al_{0.11})_{6.7}O_{21.1}\cdot Ca_{0.36}\cdot 1.51Ca(OH)_2\cdot mH_2O \quad (3)$$

Both the T/J and T/CH approaches can account for the data for the paste with 25% slag, Fig. 13. Inspection of the graphs for the paste with 50% slag (Fig. 14) shows that the TEM-EDX points for Op C–S–H are close to the positions for appropriate units (T14(2Al) and T17(2Al) that have minimum degrees of protonation, Table 4) with only a small amount of CH- or J-like structure necessary. Similarly, the data for the 75% paste (Fig. 15) are close to appropriate units (T17(3Al) and T17 (2Al) that have minimum degrees of protonation, Table 4), as are those for the 100% slag blend, Fig. 16 (long-chain Al-substituted T units with $B \approx 60\%$, and degrees of protonation between the minimum ($w = 0$) and intermediate ($w = 1$) levels).

Outer-product C–S–H can thus be envisaged to consist of interstratified layers of Al-substituted T-based structure with J- and/or CH-like structure; AFm-type (i.e. Ca–Al LDH) layers are also likely. Inner product has in addition layers of Mg–Al LDH (and probably AH_3-like structure) and we have suggested elsewhere that the very fine intermixing in the Ip region observed by TEM is due to the fact that the main layers of Mg–Al LDH and Al-substituted C–S–H are oppositely charged [8]. The contents of interlayer regions must vary considerably, depending on the local nanostructure: for example, in addition to water molecules, interlayers would contain calcium and alkali cations in Al-substituted T-based structure and a variety of anions in

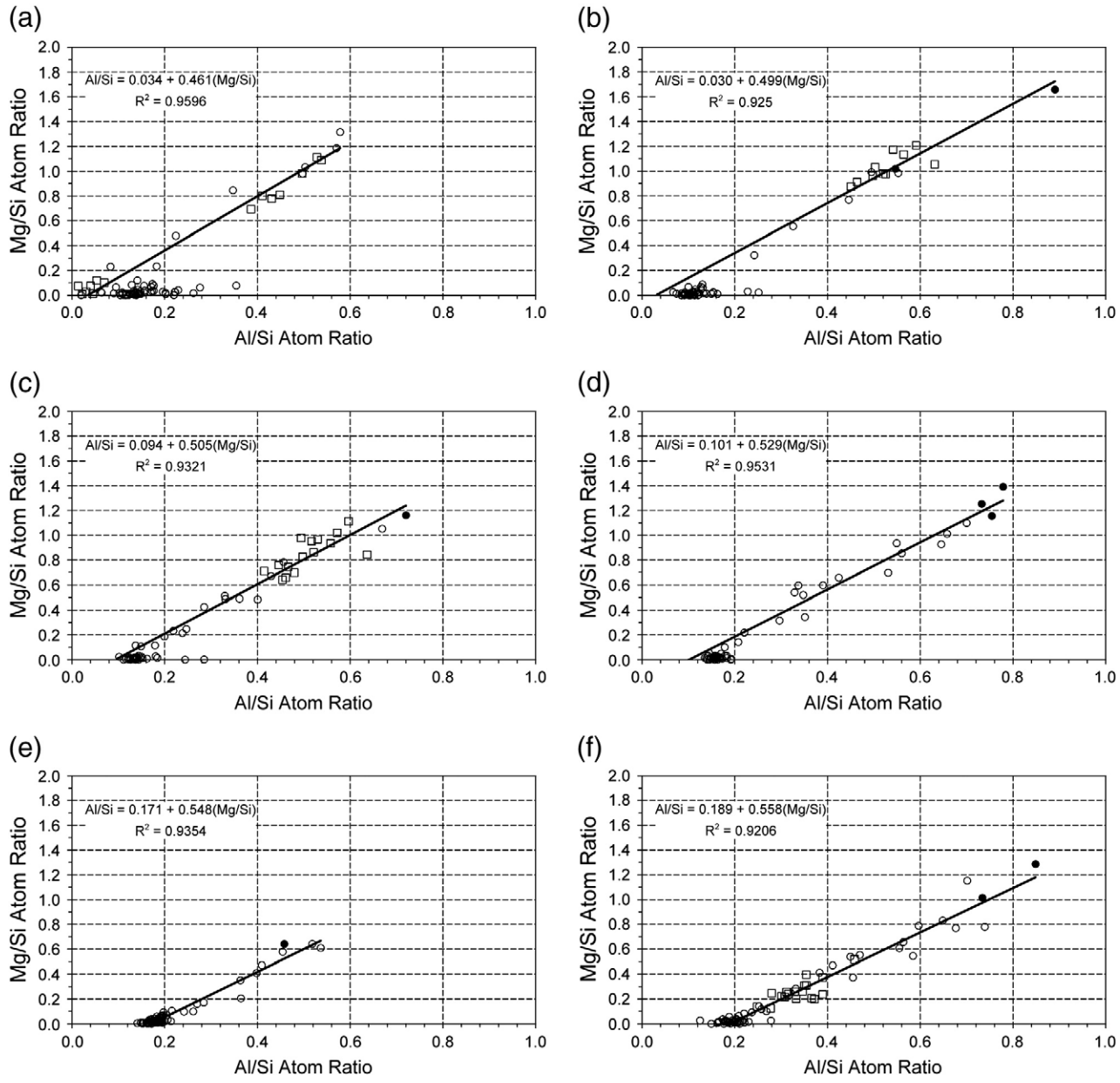

Fig. 17. Mg/Si against Al/Si atom ratio plots of TEM-EDX analyses of Op C–S–H (○), inner product (□) and hydrotalcite (●) in GGBS/OPC blends containing 10% (a), 25% (b), 50% (c), 75% (d), 90% (e) and 100% slag (f).

Ca–Al and Mg–Al LDH-based structure (or would be vacant in layers of CH- or AH_3-based structure). Whilst the interlayers of most LDH phases contain a single layer of anions and water molecules, more complex interlayer structures do occur [22], for example, double layers of anions and water molecules, such as in Mg–Al sulfate LDHs [34], and double layers of anions and cations, such as sulfate and sodium ions [35], as in the Mg–Al LDH mineral motukoreaite [36], or sulfate and magnesium ions, as in the Mg–Al LDH mineral mountkeithite [37]. It is plausible that similar complex arrangements might occur in some hardened cement pastes; for example, perhaps with sulfate and calcium ions, as in the double-layer mineral wermlandite [38], which has the formula $[Mg_7(Al_{0.57}Fe_{0.43})_2(OH)_{18}]^{2+}[(Ca_{0.6}Mg_{0.4})(SO_4)_2(H_2O)_{12}]^{2-}$.

4. Summary and conclusions

This study involved the characterization of 20-year-old slag–cement pastes and comparison of the results with data on samples from the same mixes at earlier ages, which have been published previously. The crystalline phases present in the neat cement paste included CH, AFt, hydrogarnet, a small amount of residual cement, a small amount of calcite and possibly some AFm that contains carbonate ions. The presence of the last two indicates that the neat paste was very slightly carbonated. None of the slag-containing pastes had carbonated. The blended pastes contained progressively smaller amounts of CH as the slag fraction increased, and a Mg–Al layered double hydroxide (Mg–Al LDH). The Mg/Al ratio of the Mg–Al LDH was lower than at 14 months in all cases except for the neat slag paste. ^{27}Al NMR spectra had three octahedral peaks at approximately 13, 9 and 4 ppm. The peak at 13 ppm is due to AFt and the peak at 9 ppm is probably a convolution of resonances from AFm and the Mg–Al LDH phase. The peak at 4 ppm appeared to increase as the Mg/Al ratio of the LDH phase reduced: a plausible explanation for this observation is that the 4 ppm peak is due to Al in layers of AH_3-based structure interstratified with those of the Mg–Al LDH.

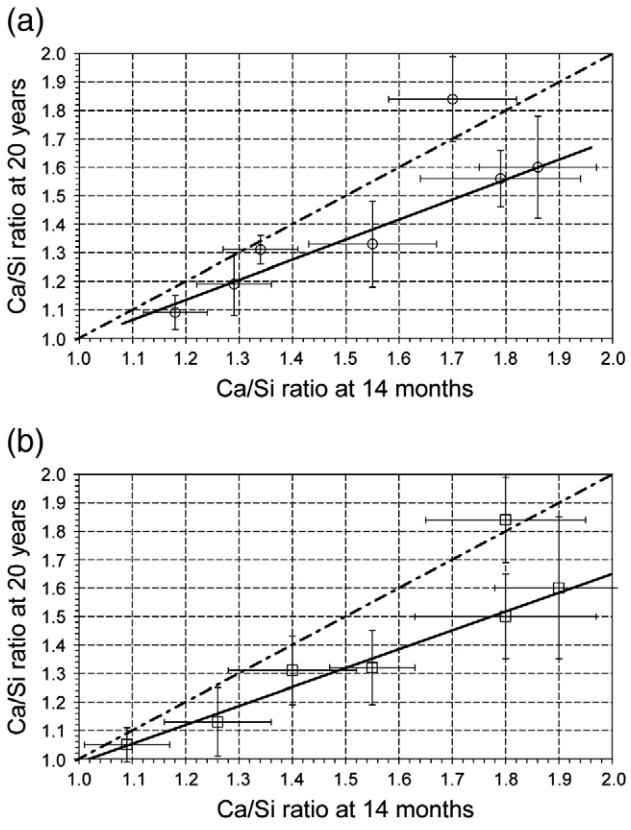

Fig. 18. Comparison of the Ca/Si atom ratio of C–S–H in GGBS/OPC blends containing 0%, 10%, 25%, 50%, 75%, 90% and 100% slag at 20 years and 14 months old. Points correspond to mean values (±1 standard deviation) determined by TEM-EDX analysis of Op C–S–H (○) and inner product (□) (slag Ip for all pastes except the neat OPC); data for the 20-year-old pastes are given in Table 4 and those for 14 months are as reported in Ref. [3]. The full lines are linear regression fits for the slag-containing blends: (a) for Op C–S–H, $Ca/Si_{20y} = 0.290 + 0.703(Ca/Si_{14m})$, $r^2 = 0.95$; (b) for inner product, $Ca/Si_{20y} = 0.325 + 0.662(Ca/Si_{14m})$, $r^2 = 0.97$.

The degree of reaction of the silicate phases in the Portland cement fraction of the pastes was high in all cases. Around two thirds of the glassy slag appeared to have reacted in the blends with ≤75% slag, about a third in the blend with 90% slag, and just a fifth in the neat slag paste. The amount of CH in the blends is consistent with additional slag reaction occurring between 2 and 20 years.

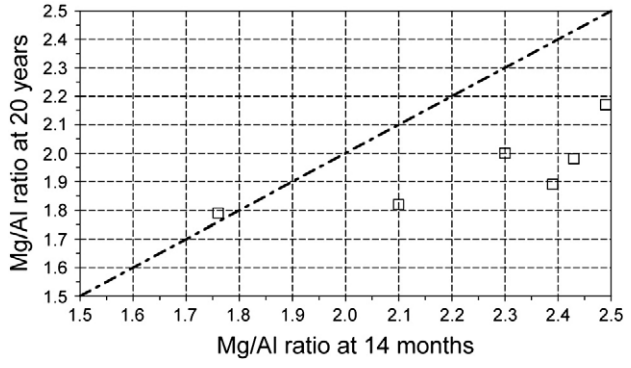

Fig. 19. Comparison of the Mg/Al ratio of the hydrotalcite-like phase (HT) at 20 years and 14 months old in GGBS/OPC blends containing 10%, 25%, 50%, 75%, 90% and 100% slag. Points correspond to values determined by TEM-EDX analysis of HT intermixed with C–S–H; data for the 20-year-old pastes are given in Table 3 and those for 14 months are as reported in Ref. [3].

Table 4
Details of selected structural units referred to in the text (see Table 1 for the definition of *B*, and Ref. [29] for *w*).

Structural unit	Degree of protonation	Si/Ca	Al/Ca	*B* (%)
T8(1Al)	Minimum, $w = 0$	0.78	0.111	50
T14(2Al)	Minimum, $w = 0$	0.80	0.133	50
T14(2Al)	Intermediate, $w = 1$	0.96	0.160	50
T17(2Al)	Minimum, $w = 0$	0.83	0.111	40
T17(3Al)	Minimum, $w = 0$	0.78	0.167	60
T17(3Al)	Intermediate, $w = 1$	0.93	0.200	60

The morphology of outer-product (Op) C–S–H appeared to be finer than at younger ages in most of the pastes; indeed, regions of Op C–S–H were sufficiently fine in most of the pastes that it was often difficult to distinguish between Op and Ip when examining the samples in the microscope. Op C–S–H was largely foil-like in the paste with 90% slag (and essentially the same as it was at 14 months) and consisted entirely of crumpled foils in the neat slag paste. The particle size-related variation in morphology of inner product (Ip) C–S–H that was noted at younger ages was still observed at 20 years: i.e. a fine, dense morphology around partly reacted grains but a coarser, foil-like morphology where there was no residual unreacted cement. The Ca/Si and Ca/(Si + Al) ratios of the Op C–S–H decreased with increasing slag content, and the Al/Si ratio increased. The Ca/Si ratio of Op C–S–H in the neat paste was higher at 20 years than at 14 months and the value for Ip C–S–H about the same. In contrast, the values for both Op and Ip C–S–H in the slag-containing pastes were all lower at 20 years than they were at 14 months; the difference is statistically significant in most cases. The mean aluminosilicate chain length of the C–S–H was very long in all the samples and would be expected to have increased with age. The positions of the TEM-EDX analyses of C–S–H on Al/Ca–Si/Ca graphs are consistent with appropriate nanostructural units in Richardson and Groves' model. Outer-product C–S–H can be envisaged to consist of interstratified layers of Al-substituted T-based structure with J- and/or CH-like structure; AFm-type (i.e. Ca–Al LDH) layers are also likely. Inner product has in addition layers of Mg–Al LDH, and probably also AH_3-like structure. The contents of interlayer regions must vary considerably, depending on the local nanostructure.

Acknowledgements

Thanks are due to the Nuclear Decommissioning Authority for financial support, to the Engineering and Physical Sciences Research Council (for funding under Grant No. GR/S45874/01 and for a studentship (RT)), and to Castle Cement and Lafarge Cements for additional technical and financial support; thanks are also due to Dr D.C. Apperley at Durham University's EPSRC-funded NMR service for collection of the ^{27}Al NMR spectra.

Table 5
Values of variables in Richardson and Groves' model for C–S–H in all the pastes calculated using the NMR and TEM-EDX data in Table 1; see Ref. [30] and references therein for details of the model. The values of *X* and *z* correspond to the minimum degree of protonation (i.e. w_{min}/n).

% GGBS	*a*	*n*	*y′*	w_{min}/n	w_{max}/n	*X*	*z*
0	0.083	2.20	4.24	0	1.76	6.60	2.47
10	0.110	2.57	2.92	0	2.00	7.70	1.51
25	0.099	2.70	3.08	0	2.00	8.10	1.46
50	0.123	4.93	2.13	0	2.00	14.80	0.33
75	0.138	5.70	1.99	0.01	2.00	17.07	0
90	0.153	5.10	1.18	0.82	2.00	13.21	0
100	0.160	∞	0.97	1.03	2.00	∞	0

References

[1] H.F.W. Taylor, Cement Chemistry, 2nd EditionThomas Telford, London, 1997.
[2] R. Taylor, I.G. Richardson, R. Brydson, Nature of C–S–H in 20 year old neat ordinary Portland cement and 10% Portland cement–90% ground granulated blast furnace slag pastes, Advanced in Applied Ceramics 106 (2007) 294–301.
[3] I.G. Richardson, G.W. Groves, The microstructure and microanalysis of hardened cement pastes involving ground granulated blast-furnace slag, Journal of Materials Science 27 (1992) 6204–6212.
[4] I.G. Richardson, G.W. Groves, The microstructure and microanalysis of hardened ordinary Portland cement pastes, Journal of Materials Science 28 (1993) 265–277.
[5] J.A. Chudek, G. Hunter, M.R. Jones, S.N. Scrimgeour, P.C. Hewlett, A.B. Kudryavtsev, Aluminium-27 solid state NMR spectroscopic studies of chloride binding in Portland cement and blends, Journal of Materials Science 35 (2000) 4275–4288.
[6] H.M. Dyson, I.G. Richardson, A.R. Brough, A combined ^{29}Si MAS NMR and selective dissolution technique for the quantitative evaluation of hydrated blast furnace slag cement, Journal of the American Ceramic Society 90 (2007) 598–602.
[7] I.G. Richardson, S.A. Rodger, G.W. Groves, The microstructure of GGBFS/OPC hardened cement pastes and some effects of leaching, Materials Research Society Symposia Proceedings 176 (1990) 63–74.
[8] I.G. Richardson, The nature of C–S–H in hardened cements, Cement and Concrete Research 29 (1999) 1131–1147.
[9] I. Klur, B. Pollet, J. Virlet, A. Nonat, C–S–H structure evolution with calcium content by multinuclear NMR, in: P. Colombet, A.-R. Grimmer, H. Zanni, P. Sozzani (Eds.), Nuclear Magnetic Resonance Spectroscopy of Cement Based Materials, Bergamo, Italy, Springer-Verlag, 1998, pp. 119–141.
[10] I.G. Richardson, The nature of the hydration products in hardened cement pastes, Cement and Concrete Composites 22 (2000) 97–113.
[11] I.G. Richardson, G.W. Groves, The structure of the calcium silicate hydrate phases present in hardened pastes of white Portland cement/blast-furnace slag blends, Journal of Materials Science 31 (1997) 4793–4802.
[12] K.J.D. Mackenzie, M.E. Smith, Multinuclear Solid-State NMR of Inorganic materials, vol. 6, Pergamon, Amsterdam; London, 2002.
[13] I.G. Richardson, A.R. Brough, G.W. Groves, C.M. Dobson, The characterization of hardened alkali-activated blast-furnace slag pastes and the nature of the calcium silicate hydrate (C–S–H) phase, Cement and Concrete Research 24 (1994) 813–829.
[14] J. Schneider, M.A. Cincotto, H. Panepucci, Si-29 and Al-27 high-resolution NMR characterization of calcium silicate hydrate phases in activated blast-furnace slag pastes, Cement and Concrete Research 31 (2001) 993–1001.
[15] J. Skibsted, E. Henderson, H.J. Jakobsen, Characterization of calcium aluminate phases in cements by ^{27}Al MAS NMR spectroscopy, Inorganic Chemistry 32 (1993) 1013–1027.
[16] M.D. Andersen, H.J. Jakobsen, J. Skibsted, Incorporation of aluminum in the calcium silicate hydrate (C–S–H) of hydrated Portland cements: a high-field ^{27}Al and ^{29}Si MAS NMR investigation, Inorganic Chemistry 42 (2003) 2280–2287.
[17] F. Rey, V. Fornes, J.M. Rojo, Thermal decomposition of hydrotalcites — an infrared and nuclear magnetic resonance spectroscopic study, Journal of the Chemical Society — Faraday Transactions 88 (1992) 2233–2238.
[18] K. Takehira, T. Kawabata, S. Shishido, K. Murakami, T. Ohi, D. Shoro, M. Honda, K. Takaki, Mechanism of reconstitution of hydrotalcite leading to eggshell-type Ni loading on Mg–Al mixed oxide, Journal of Catalysis 231 (2005) 92–104.
[19] M.A. Aramendía, Y. Avilés, V.B. Borau, J.M. Luque, J.M. Marinas, J.R. Ruiz, F.J. Urbano, Thermal decomposition of Mg/Al and Mg/Ga layered-double hydroxides: a spectroscopic study, Journal of Materials Chemistry 9 (1999) 1603–1607.
[20] M.D. Andersen, H.J. Jakobsen, J. Skibsted, A new aluminium hydrate species in hydrated Portland cements characterized by ^{27}Al and ^{29}Si MAS NMR spectroscopy, Cement and Concrete Research 36 (2006) 3–17.
[21] G.W. Brindley, S. Kikkawa, A crystal-chemical study of Mg,Al and Ni, Al hydroxy-perchlorates and hydroxy-carbonate, American Mineralogist 64 (1979) 836–843.
[22] D.G. Evans, R.C.T. Slade, Structural aspects of layered double hydroxides, Structure and Bonding 119 (2006) 1–87.
[23] A.V. Arakcheeva, D.Y. Pushcharovskii, R.K. Rastsvetaeva, D. Atencio, G.U. Lubman, Crystal structure of comparative crystal chemistry of $Al_2Mg_4(OH)_{12}(CO_3)\cdot 3H_2O$, a new mineral from the hydrotalcite–manasseite group, Krystallografiya 41 (1996) 1024–1034.
[24] H. Saafeld, M. Wedde, Refinement of crystal structure of gibbsite, $Al(OH)_3$, Zeitschrift für Kristallographie 139 (1974) 129–135.
[25] D.E. Woessner, Characterization of clay minerals by ^{27}Al nuclear magnetic resonance spectroscopy, American Mineralogist 74 (1989) 203–215.
[26] R.C.T. Slade, J.C. Southern, I.M. Thompson, ^{27}Al nuclear magnetic resonance spectroscopy investigation of thermal transformation sequences of alumina hydrates: Part 1. Gibbsite, γ-$Al(OH)_3$, Journal of Materials Chemistry 1 (1991) 563–568.
[27] P. Faucon, A. Delagrave, J.C. Petit, C. Richet, J.M. Marchand, H. Zanni, Aluminum incorporation in calcium silicate hydrates (C–S–H) depending on their Ca/Si ratio, Journal of Physical Chemistry B 103 (1999) 7796–7802.
[28] G.K. Sun, J.F. Young, R.J. Kirkpatrick, The role of Al in C–S–H: NMR, XRD, and compositional results for precipitated samples, Cement and Concrete Research 36 (2006) 18–29.
[29] I.G. Richardson, G.W. Groves, The incorporation of minor and trace elements into calcium silicate hydrate (C–S–H) gel in hardened cement pastes, Cement and Concrete Research 23 (1993) 131–138.
[30] I.G. Richardson, Tobermorite/jennite- and tobermorite/calcium hydroxide-based models for the structure of C–S–H: applicability to hardened pastes of tricalcium silicate, β-dicalcium silicate, Portland cement, and blends of Portland cement with blast-furnace slag, metakaolin, or silica fume, Cement and Concrete Research 34 (2004) 1733–1777.
[31] A.V. Girão, I.G. Richardson, R.M.D. Brydson, Composition, morphology and nanostructure of C–S–H in white Portland cement–fly ash blends hydrated at 85 °C, Advances in Applied Ceramics 106 (2007) 283–293.
[32] C.A. Love, I.G. Richardson, A.R. Brough, Composition and structure of C–S–H in white Portland cement–20% metakaolin pastes hydrated at 25 °C, Cement and Concrete Research 37 (2007) 109–117.
[33] I.G. Richardson, The calcium silicate hydrates, Cement and Concrete Research 38 (2008) 137–158.
[34] G.W. Brindley, S. Kikkawa, Thermal behaviour of hydrotalcite and of anion-exchanged forms of hydrotalcite, Clays and Clay Minerals 28 (1980) 87–91.
[35] V.A. Drits, T.N. Sokolova, G.V. Sokolova, V.I. Cherkashin, New members of the hydrotalcite–manasseite group, Clays and Clay Minerals 35 (1987) 401–417.
[36] J. Ruis, F. Plana, Contribution to the superstructure resolution of the double-layer mineral motukoreaite, Neues Jahrbuch fur Mineralogie-Monatshefte 6 (1986) 263–272.
[37] D.R. Hudson, M. Bussell, Mountkeithite, a new pyroaurite-related mineral with an expanded interlayer containing exchangeable $MgSO_4$, Mineralogical Magazine 44 (1981) 345–350.
[38] J. Ruis, R. Allmann, The superstructure of the double-layer mineral wermlandite $[Mg_7(Al_{0.57}Fe_{0.43})_2(OH)_{18}]^{2+}[(Ca_{0.6}Mg_{0.4})(SO_4)_2(H_2O)_{12}]^{2-}$, Zeitschrift für Kristallographie 168 (1984) 133–144.